Time Refraction of Spin Waves

K. Schultheiss,[1,*] N. Sato,[1] P. Matthies,[1,2] L. Körber,[1,2] K. Wagner,[1] T. Hula,[1] O. Gladii,[1] J. E. Pearson,[3] A. Hoffmann,[3,†] M. Helm,[1,2] J. Fassbender,[1,2] and H. Schultheiss[1,2]

[1]*Helmholtz-Zentrum Dresden - Rossendorf, Institute of Ion Beam Physics and Materials Research, 01328 Dresden, Germany*
[2]*Fakultät Physik, Technische Universität Dresden, 01062 Dresden, Germany*
[3]*Materials Science Division, Argonne National Laboratory, Argonne, Illinois 60439, USA*

(Received 9 September 2020; accepted 4 March 2021; published 30 March 2021)

We present an experimental study of time refraction of spin waves (SWs) propagating in microscopic waveguides under the influence of time-varying magnetic fields. Using space- and time-resolved Brillouin light scattering microscopy, we demonstrate that the broken translational symmetry along the time coordinate results in a loss of energy conservation for SWs and thus allows for a broadband and controllable shift of the SW frequency. With an integrated design of SW waveguide and microscopic current line for the generation of strong, nanosecond-long, magnetic field pulses, a conversion efficiency up to 39% of the carrier SW frequency is achieved, significantly larger compared to photonic systems. Given the strength of the magnetic field pulses and its strong impact on the SW dispersion relation, the effect of time refraction can be quantified on a length scale comparable to the SW wavelength. Furthermore, we utilize time refraction to excite SW bursts with pulse durations in the nanosecond range and a frequency shift depending on the pulse polarity.

DOI: 10.1103/PhysRevLett.126.137201

The manipulation of waves can be achieved by modulating the properties of the medium in which the wave propagates either in space or in time. Changes along the space coordinates affect the momentum of the wave due to the lost translational invariance of space but conserve the energy of the wave. Well-known examples are the diffraction of waves at opaque obstacles or the refraction of light according to Snell's law. While these phenomena are classified by the term "space refraction," its counterpart is known as "time refraction," which conserves the momentum of the wave but changes its energy due to the lost translational invariance of time [1]. A key requirement for time refraction is to temporarily change the medium parameters, which affect the dispersion relation of the wave, in an adiabatic manner, i.e., slower than the oscillation period of the wave but faster than its lifetime. Recently, Zhou *et al.* reported on the experimental observation of time refraction of photons using a subwavelength-thick indium tin oxide film in its epsilon-near-zero (ENZ) spectral range [2]. Making use of the strong nonlinear light-matter interactions in the ENZ state, the authors were able to reach frequency conversion efficiencies up to 6% of the carrier frequency, clearly exceeding previous works reporting efficiencies around 0.145% [3]. At the same time, Zhou *et al.* kept the interaction length of photons and refractive medium smaller than the photon wavelength, which is especially challenging in photonic systems. In ferromagnets, however, which host spin waves (SWs) as collective excitations of the spin system, the strong coupling of SWs to the magnetic field and their rather small phase velocity compared to the speed of light allows for even higher relative frequency shifts and a full spatiotemporal study of time refraction.

The dispersion relation of SWs depends strongly on the effective magnetic field, the magnitude and direction of the magnetization, and the thickness and lateral dimensions of the SW waveguide [4]. Typically, SWs have frequencies in the gigahertz range and their phase and group velocities are comparable to the speed of sound in solids. Space refraction of SWs was already demonstrated in the last two decades for spatially inhomogeneous magnetic fields [5], changes of the waveguide width [6], spatial variations of the magnetization generated by heat gradients [7], directional changes of the magnetization [8,9], and thickness variations along the SW propagation path [10,11]. In all these studies, changes of the SW momenta were reported under conservation of the SW energy. However, there are only few reports on time refraction of SWs in macroscopic yttrium-iron-garnet waveguides dating back up to 50 years [12–14]. Given the lack of spatially resolved methods for mapping SW propagation at that time, these studies could only analyze the change of the SW energy after propagation of 1 cm. These experiments demonstrated frequency shifts without significant distortions of the SW pulse up to 90 MHz for a carrier frequency of 1.2 GHz, yielding a conversion efficiency of 7.5%.

In this Letter, we report on micron sized SW waveguides with integrated current lines for generating large and rapidly changing magnetic fields using current pulses. For the first time, we present a full spatiotemporal

quantification of time refraction of SWs using time-resolved Brillouin light scattering (TR-μBLS) microscopy [15]. We demonstrate relative changes of the SW frequency up to 39% over propagation distances comparable to the SW wavelength. Depending on the polarity of the dc pulses, the SW energy can be increased or decreased within a few nanoseconds.

The experimental layout is shown in Fig. 1. We pattern a ferromagnetic $Ni_{81}Fe_{19}$ waveguide (width $w = 2$ μm, thickness $t = 30$ nm) on top of a Cr(10 nm)/Au(25 nm) conduction line ($w = 3.2$ μm), as can be seen in the scanning electron micrograph in Fig. 1. A current pulse flowing in the conduction line generates a pulsed Oersted field $\boldsymbol{H}_{\mathrm{Oe}}$, which is aligned either parallel or antiparallel to the direction of an external magnetic field $\boldsymbol{H}_{\mathrm{ext}}$, depending on the polarity of the current pulse. This allows for a rapid change of the total magnetic field inside the $Ni_{81}Fe_{19}$ waveguide. Note that the broadening of the Au conduction line in y direction is not relevant for this study since all measurements were performed in the 6.4 μm-long part before the broadening begins.

A microwave current flowing through a CPW (see Fig. 1) excites SWs with a fixed frequency $f_{\mathrm{rf}} = 3.65$ GHz and a preferential wave vector $k_{\mathrm{max}} = 1.04$ rad/μm. The shaded area in Fig. 2 plots the normalized excitation efficiency of the CPW on a linear scale to illustrate its wave vector dependence. It is calculated via a fast Fourier transform of the Oersted field generated by the currents flowing in the CPW. To determine the resonance field for these specific excitation conditions, we use BLS microscopy to measure the SW intensity in 1 μm distance to the CPW as a function of the external magnetic field H_{ext}, without applying any dc current pulses. As can be seen from the results in Fig. 2(a), SWs are excited most efficiently at the resonance field $\mu_0 H_{\mathrm{res}} = 22.4$ mT.

In order to compare this to the dispersion relation, we need to take into account the strong influence of the demagnetizing field and the quantization of the SW wave vector across the waveguide width. Therefore, we simulate the static magnetization inside the waveguide for external fields between 10 and 50 mT using MuMax^3[16,17]. Black squares in Fig. 2(b) show the effective field B_{eff}, which is determined in the center of the waveguide. The effective quantization width w_{eff} is given by red triangles in Fig. 2(b) and is derived from the positions at which the y component of the magnetization reaches 99% of the saturation magnetization $m_y = 0.99 M_S$. For $H_{\mathrm{ext}} \leq H_{\mathrm{crit}} = 14$ mT, the external field is too weak to compensate the demagnetizing fields so that the magnetization is aligned predominantly along the waveguide.

Based on the results for B_{eff} and w_{eff}, we plot dispersion relations for various magnetic fields $16 \leq \mu_0 H_{\mathrm{tot}} \leq 50$ mT in Fig. 2(c). The calculations follow the formalism of Kalinikos and Slavin [4], taking into account the quantization of the wave vector across the waveguide width $k_y = \pi / w_{\mathrm{eff}}$ and using the same material parameters as in the micromagnetic simulations [17]. The excitation conditions for SWs in our system ($f_{\mathrm{rf}} = 3.65$ GHz, $k_{\mathrm{max}} = 1.04$ rad/μm) match the dispersion calculated for $\mu_0 H_{\mathrm{ext}} = 22$ mT [thicker green line in Fig. 2(c)], which is in good agreement with the measured resonance field $\mu_0 H_{\mathrm{res}} = 22.4$ mT.

First, we demonstrate the influence of the pulsed Oersted fields in TR-μBLS measurements of the thermal SW signal. Figure 2(d) shows the temporal evolution of the thermal SW spectrum for $\mu_0 H_{\mathrm{ext}} = 22.4$ mT with the BLS intensity color coded. Up to $t = 0$ ns, only the external field determines the SW frequencies with a minimum at 3.0 GHz. At $t = 0$ ns, a current pulse is applied with 20 ns duration, 3 ns rise and fall time, and amplitude $I_{\mathrm{dc}} = 64.2$ mA. Inside the $Ni_{81}Fe_{19}$ waveguide, this generates an Oersted field $\mu_0 H_{\mathrm{Oe}} = 12.2$ mT, which is aligned parallel to the external field and thus increases the overall magnetic field. Hence, in this 20 ns window, the SW spectrum is shifted to higher frequencies rising at around 4.6 GHz. To better visualize this shift, we integrate the BLS intensity inside (dc on) and outside (dc off) the 20 ns window and plot both spectra in Fig. 2(e). The frequencies of the rising flanks of the spectra measured without (3.0 GHz) and with (4.6 GHz) additional dc pulse are in excellent agreement with the onsets of the dispersion relation at $\mu_0 H_{\mathrm{tot}} = 22.4$ and 34.6 mT, respectively.

In a next step, we study how SWs adapt to temporal changes of the magnetic field if a continuous microwave signal is applied to the CPW at $f_{\mathrm{rf}} = 3.65$ GHz. Therefore, we distinguish different sequences of time-varying magnetic fields: the external magnetic field matches the resonance condition so that any additional dc pulse shifts SWs out of resonance [see arrows A and B in Fig. 2(a)] or the initial external magnetic field is larger than the

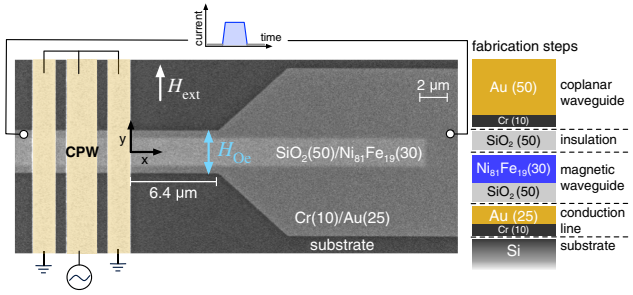

FIG. 1. Scanning electron microscopy (SEM) image of the investigated structure. A $Ni_{81}Fe_{19}$ waveguide (width $w = 2$ μm, thickness $t = 30$ nm) is fabricated on top of a Cr(10 nm)/Au(25 nm) conduction line ($w = 3.2$ μm), insulated by 50 nm SiO_2. SWs are excited by a coplanar waveguide (CPW) and propagate along the $+x$ direction, with $x = 0$ μm defined by the right edge of the CPW. An external magnetic field $\boldsymbol{H}_{\mathrm{ext}}$ is applied along the $+y$ direction. Fabrication steps on the right highlight the insulation layers, which are not visible in the SEM image.

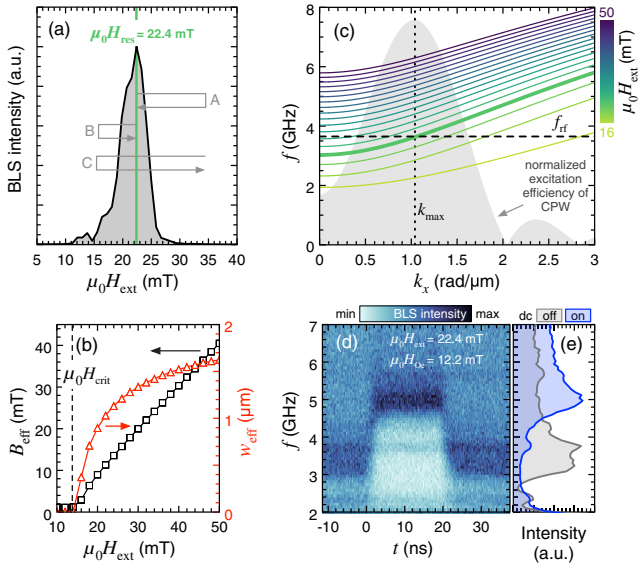

FIG. 2. (a) BLS intensity measured for SWs excited at $f_{rf} = 3.65$ GHz as a function of the externally applied field. The arrows A–C depict different sequences of the time-varying magnetic fields. (b) Effective field B_{eff} and effective localization width w_{eff} determined from micromagnetic simulations for different external magnetic fields. (c) Dispersion relations calculated considering the resulting B_{eff} and w_{eff} as in (b). The dotted vertical line indicates the wave vector k_{max}, which is excited most efficiently by the CPW. The horizontal dashed line indicates the excitation frequency f_{rf}, fixed in all measurements at 3.65 GHz. (d) BLS measurement of the thermal SW intensity as a function of frequency and time with the BLS intensity color coded. (e) Frequency spectra integrated in time windows when the dc pulse is on and off, respectively.

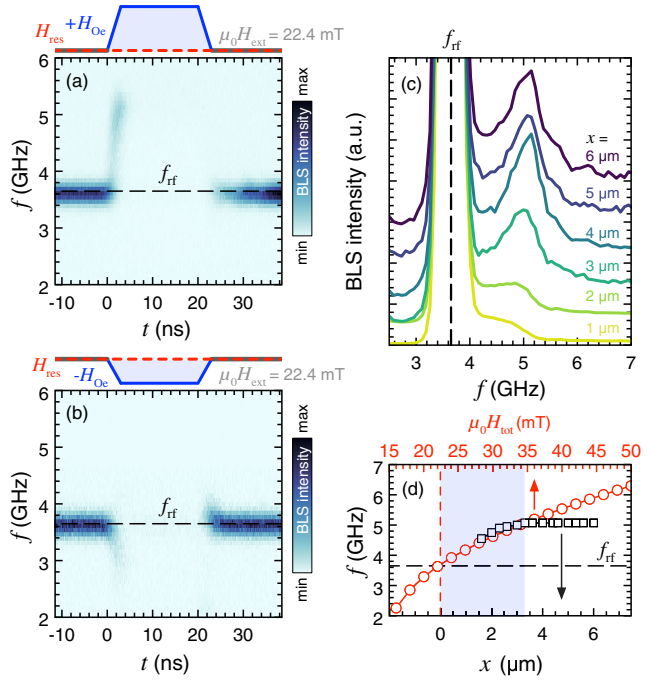

FIG. 3. TR-BLS signal measured at $x = 4$ μm for (a) $\boldsymbol{H}_{Oe}\uparrow\uparrow\boldsymbol{H}_{ext}$ with $\mu_0 H_{Oe} = 12.2$ mT and (b) $\boldsymbol{H}_{Oe}\uparrow\downarrow\boldsymbol{H}_{ext}$ with $\mu_0 H_{Oe} = 6.8$ mT. The excitation was fixed at $f_{rf} = 3.65$ GHz (horizontal dashed lines). (c) SW intensities integrated over all times and measured at different distances x to the edge of the CPW. Plots for different x are drawn with different intensity offsets to separate the plots vertically and thus increase readability. (d) Frequencies measured for the shifted SW peak as function of x (black squares) compared to frequencies calculated from the dispersion relation for the wave vector $k_{max} = 1.04$ rad/μm as function of the total magnetic field (red circles). The light blue area highlights the field range covered by the dc pulse.

resonance field, and the dc pulse is injected so that the associated Oersted field reduces the total magnetic field to cross the resonance condition [see arrow C in Fig. 2(a)].

We start with the case when the external field is set to the resonance field $\mu_0 H_{ext} = \mu_0 H_{res} = 22.4$ mT and the dc pulse generates an Oersted field $\mu_0 H_{Oe} = 12.2$ mT parallel to the external field [arrow A in Fig. 2(a)]. The pulse duration is 20 ns with 3 ns rise and fall time. Figure 3(a) shows the corresponding intensity plot of the μBLS signal, which was measured in $x = 4$ μm distance from the edge of the CPW. Up to $t = 0$ ns, i.e., before injecting the dc pulse, a strong BLS signal is detected at 3.65 GHz, as expected for resonant excitation.

During the 3 ns rise time of the dc pulse, we detect a rapid increase of the SW frequency. This frequency shift is due to the parallel alignment of external field and Oersted field $\boldsymbol{H}_{Oe}\uparrow\uparrow\boldsymbol{H}_{ext}$, which causes an increase of the total magnetic field H_{tot} and shifts the dispersion to higher frequencies. However, unlike in the case of thermal SWs, the SW signal vanishes shortly after the dc pulse sets in. Only as long as $\mu_0 H_{tot} = \mu_0 H_{res} = 22.4$ mT (i.e., $t < 0$ ns), SWs are resonantly excited by the CPW. With the additional Oersted field, $H_{tot} > H_{res}$ and no more SWs can be excited at $f_{rf} = 3.65$ GHz. Only those SWs that were excited before the dc pulse sets in and are still propagating along the waveguide experience the changing magnetic field and adjust their frequency due to time refraction. Naturally, after the dc pulse is switched off, the total magnetic field matches the resonance condition and SWs can be excited again.

If we keep the external field to match the resonance condition $\mu_0 H_{ext} = \mu_0 H_{res} = 22.4$ mT but reverse the direction of the Oersted field [arrow B in Fig. 2(a)] with reduced amplitude $\mu_0 H_{Oe} = 6.8$ mT, the result is similar. Now, $\boldsymbol{H}_{Oe}\uparrow\downarrow\boldsymbol{H}_{ext}$ so that the total field is reduced during the dc pulse and the SW frequency shifts to lower values during the rise time of the pulse, as can be seen in Fig. 3(b). Note that this results in $H_{tot} < H_{crit}$ [see Fig. 2(b)], which does not suffice to saturate even parts of the waveguide along its short axis. Hence, SW propagation is less efficient and the shifted signal in Fig. 3(b) is much weaker compared to Fig. 3(a).

So far, we detected SWs only in one fixed position. Now, we analyze the amplitude of the frequency shift as a

function of the propagation distance x. In Fig. 3(c), we plot the μBLS intensity integrated over time that was measured at different positions x for $\boldsymbol{H}_{\mathrm{Oe}}\uparrow\uparrow\boldsymbol{H}_{\mathrm{ext}}$ with $\mu_0 H_{\mathrm{ext}} = 22.4$ and $\mu_0 H_{\mathrm{Oe}} = 12.2$ mT. Each plot shows two peaks: one peak at 3.65 GHz, which is associated with resonant excitation when the dc pulse is still off and is cut off in the plot due to its very high intensity, and a second peak with much lower intensities at higher frequencies showing SWs that are shifted due to time refraction. Since we are interested only in the frequencies of the shifted peaks, we focus our plot on the lower intensity range and chose different intensity offsets for different x to separate the plots vertically and increase readability. As can be seen, the frequency shift increases gradually and does not change for $x \geq 4$ μm.

In Fig. 3(d), black squares plot the shifted frequencies as a function of x. To compare our data to the dispersion relation, red circles show the frequencies that were calculated for $k_{\mathrm{max}} = 1.04$ rad/μm from the dispersion relation in Fig. 2(c). To match the different x axes for both sets of data, we have to consider that only propagating SWs adjust to the changing field and propagation from the antenna to position x needs a certain amount of time. This means, at $x = 0$ μm, SWs are detected directly where they are excited and cannot be affected by any changes of the magnetic field. Hence, the field still matches the externally applied field $\mu_0 H_{\mathrm{ext}} = 22.4$ mT. When measuring at $x > 0$ μm, SWs propagate in the changing field for a few nanoseconds and adjust their frequency before they are detected. As soon as SWs propagate longer than 3 ns, which equals the rise time of the dc pulse, the frequency shift does not increase any more because the maximum Oersted field is reached already. In our experiment, this is the case for $x \geq 3.3$ μm where the detected frequency shift reaches its maximum value of 1.42 GHz. This corresponds to 39% relative frequency shift due to time refraction. Up to the point where the measured data reach the plateau, measured and calculated frequencies are in excellent agreement.

Now we consider the case when the initial external magnetic field is larger than the resonance field and the dc pulse is injected to generate an Oersted field that reduces the effective field to cross the resonance condition [arrow C in Fig. 2(a)]. Figure 4(a) shows the BLS intensity for $\boldsymbol{H}_{\mathrm{Oe}}\uparrow\downarrow\boldsymbol{H}_{\mathrm{ext}}$ with $\mu_0 H_{\mathrm{ext}} = 34.5$ and $\mu_0 H_{\mathrm{Oe}} = 19.0$ mT. Only for two short moments in time, during the rise and fall time of the dc pulse, SW bursts are detected. Only at these times, the total field matches the resonance field $\mu_0 H_{\mathrm{tot}} = \mu_0 H_{\mathrm{res}} = 22.4$ mT and allows for the excitation of SW bursts with $f_{\mathrm{rf}} = 3.65$ GHz. However, the SW bursts are not detected at 3.65 GHz but at lower (higher) values at the rising (falling) edge of the dc pulse, respectively. This is related to the still changing total magnetic field while the SW bursts propagate. At the rising edge of the dc pulse, the total field continues to reduce, leading to a downshift of the burst frequency. At the falling edge, the total field still increases, resulting in a higher average frequency of the SW burst.

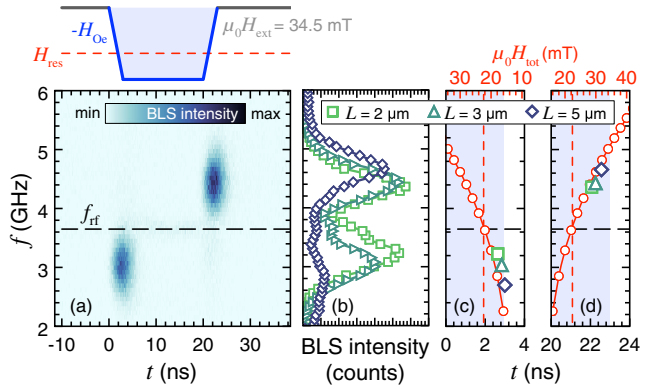

FIG. 4. (a) Time-resolved BLS signal measured at $x = 3$ μm for $\boldsymbol{H}_{\mathrm{Oe}}\uparrow\downarrow\boldsymbol{H}_{\mathrm{ext}}$ with $\mu_0 H_{\mathrm{ext}} = 34.5$ and $\mu_0 H_{\mathrm{Oe}} = 19.0$ mT. The excitation frequency was fixed to $f_{\mathrm{rf}} = 3.65$ GHz (horizontal dashed line). (b) BLS spectra integrated over time for different x with the same field configuration as in (a). (c),(d) Frequencies and detection times of the SW bursts measured at different x for (c) the rising edge of the dc pulse and (d) the falling edge. The 3 ns rise and fall time are highlighted in light blue.

Figure 4(b) shows the BLS intensity integrated over time and measured at different distances x to the antenna. Moving away from the antenna, the frequency shifts of the SW bursts increase, similar to our observations for resonant excitation discussed above. The larger the propagation distance, the longer the bursts propagate in the time-varying field and hence the more their frequencies are shifted.

To compare this with calculations of the dispersion, the frequencies of the SW bursts are plotted as a function of time in Fig. 4(c) for the rising edge of the dc pulse and in Fig. 4(d) for the falling edge. Red circles show the frequencies that were calculated from the dispersion for $k_{\mathrm{max}} = 1.04$ rad/μm as a function of the total magnetic field (upper x axis). To match both x axes, we have to consider that, for the rising edge of the dc pulse, the total field at $t = 0$ ns still matches the externally applied field: $\mu_0 H_{\mathrm{tot,0\ ns}} = 34.5$ mT. After 3 ns rise time, the pulse amplitude reaches its maximum, which yields $\mu_0 H_{\mathrm{Oe}} = 19.0$ and $\mu_0 H_{\mathrm{tot,3\ ns}} = 15.5$ mT. As can be seen in Fig. 4(c), the measured frequencies of the SW bursts nicely coincide with what is expected from theory. For the falling edge of the dc pulse [Fig. 4(d)], the axis of the total magnetic field is simply reversed, i.e., $\mu_0 H_{\mathrm{tot,20\ ns}} = 15.5$ mT and $\mu_0 H_{\mathrm{tot,23\ ns}} = 34.5$ mT. Experimental data and theoretical calculations match well.

In conclusion, we have experimentally quantified time refraction of SWs in combined space- and time-resolved studies of SW propagation in rapidly changing magnetic fields. We demonstrated the acceleration and deceleration of SWs with frequencies in the gigahertz range on length scales comparable to the SW wavelength. The prospect of

manipulating SW frequencies on such short time and length scales is of fundamental importance for hybrid quantum systems in which magnons, the quanta of SWs, are considered as strongly localized and tunable microwave sources to pump and control solid-state qubits [18,19].

This work was supported by the Deutsche Forschungsgemeinschaft within program SCHU 2922/1-1. K. S. acknowledges funding within the Helmholtz Postdoc Programme. Discussions with A. N. Slavin are gratefully acknowledged. We thank Attila Kákay for his support in micromagnetic simulations. Samples were prepared at the Argonne National Laboratory with thin film growth supported by the U.S. Department of Energy, Office of Science, Materials Science and Engineering Division. Lithography was performed at the Center for Nanoscale Materials, an Office of Science user facility, which was supported by the U.S. Department of Energy, Office of Science, Basic Energy Sciences, under Award No. DE-AC02-06CH11357.

*k.schultheiss@hzdr.de
†Permanent address: Department of Materials Science and Engineering, University of Illinois at Urbana-Champaign, Urbana, Illinois 61801, USA.

[1] J. T. Mendonça, A. Guerreiro, and A. M. Martins, Phys. Rev. A **62**, 033805 (2000).
[2] Y. Zhou, M. Z. lam, M. Karimi, J. Upham, O. Reshef, C. Liu, A. E. Willner, and R. W. Boyd, Nat. Commun. **11**, 2180 (2020).
[3] S. F. Preble, Q. Xu, and M. Lipson, Nat. Photonics **1**, 293 (2007).
[4] B. A. Kalinikos and A. N. Slavin, J. Phys. C **19**, 7013 (1986).
[5] A. V. Chumak, T. Neumann, A. A. Serga, B. Hillebrands, and M. P. Kostylev, J. Phys. D **42**, 205005 (2009).
[6] V. E. Demidov, M. P. Kostylev, K. Rott, J. Münchenberger, G. Reiss, and S. O. Demokritov, Appl. Phys. Lett. **99**, 082507 (2011).
[7] B. Obry, V. I. Vasyuchka, A. V. Chumak, A. A. Serga, and B. Hillebrands, Appl. Phys. Lett. **101**, 192406 (2012).
[8] K. Vogt, F. Y. Fradin, J. E. Pearson, T. Sebastian, S. D. Bader, B. Hillebrands, A. Hoffmann, and H. Schultheiss, Nat. Commun. **5**, 3727 (2014).
[9] S.-K. Kim, S. Choi, K.-S. Lee, D.-S. Han, D.-E. Jung, and Y.-S. Choi, Appl. Phys. Lett. **92**, 212501 (2008).
[10] J. Stigloher, M. Decker, H. S. Körner, K. Tanabe, T. Moriyama, T. Taniguchi, H. Hata, M. Madami, G. Gubbiotti, K. Kobayashi, T. Ono, and C. H. Back, Phys. Rev. Lett. **117**, 037204 (2016).
[11] J. N. Toedt, S. Mansfeld, D. Mellem, W. Hansen, D. Heitmann, and S. Mendach, Phys. Rev. B **93**, 184416 (2016).
[12] S. M. Rezende and F. R. Morgenthaler, Appl. Phys. Lett. **10**, 184 (1967).
[13] B. A. Auld, J. H. Collins, and H. R. Zapp, Appl. Phys. Lett. **10**, 186 (1967).
[14] V. L. Preobrazhenskii and Y. K. Fetisov, Sov. Phys. J. **31**, 898 (1988).
[15] T. Sebastian, K. Schultheiss, B. Obry, B. Hillebrands, and H. Schultheiss, Front. Phys. **3**, 35 (2015).
[16] A. Vansteenkiste, J. Leliaert, M. Dvornik, M. Helsen, F. Garcia-Sanchez, and B. Van Waeyenberge, AIP Adv. **4**, 107133 (2014).
[17] The dispersion relation and micromagnetic simulations were performed using the following material parameters: saturation magnetization $M_s = 830$ kA/m, reduced gyromagnetic ratio $\gamma/2\pi = 28$ GHz/T, exchange constant $A = 13$ pJ/m.
[18] P. Andrich, C. F. de las Casas, X. Liu, H. L. Bretscher, J. R. Berman, F. J. Heremans, P. F. Nealey, and D. D. Awschalom, npj Quantum Inf. **3**, 28 (2017).
[19] Y. Li, W. Zhang, V. Tyberkevych, W.-K. Kwok, A. Hoffmann, and V. Novosad, J. Appl. Phys. **128**, 130902 (2020).